Science Advances
AAAS

Supplementary Materials for

Mitochondrial C1qbp promotes differentiation of effector CD8$^+$ T cells via metabolic-epigenetic reprogramming

Xingyuan Zhai, Kai Liu, Hongkun Fang, Quan Zhang, Xianjun Gao, Fang Liu, Shangshang Zhou, Xinming Wang, Yujia Niu, Yazhen Hong, Shu-Hai Lin, Wen-Hsien Liu, Changchun Xiao, Qiyuan Li*, Nengming Xiao*

*Corresponding author. Email: qiyuan.li@xmu.edu.cn (Q.L.); nengming@xmu.edu.cn (N.X.)

Published 3 December 2021, *Sci. Adv.* **7**, eabk0490 (2021)
DOI: 10.1126/sciadv.abk0490

The PDF file includes:

Figs. S1 to S9

Other Supplementary Material for this manuscript includes the following:

Tables S1 and S2

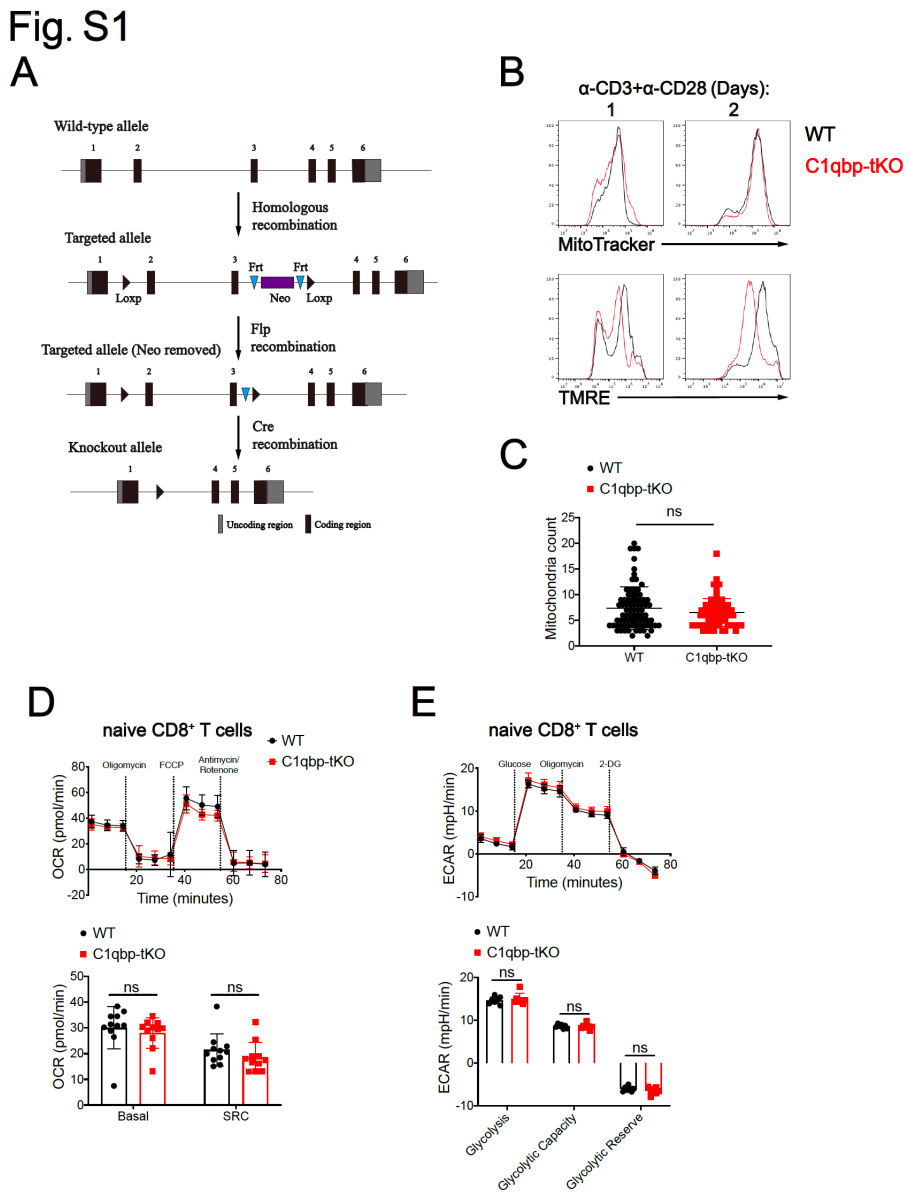

Fig. S1. C1qbp is dispensable for mitochondrial OXPHOS in naive CD8⁺ T cells. **(A)** Strategy for *C1qbp* gene targeting. **(B)** Mitochondrial mass and mitochondrial membrane potential (MMP) were measured by MitoTracker Deep Red (MTDR) staining and TMRE staining respectively, in activated CD8⁺ T cells at indicated days. **(C)** Quantification of numbers of mitochondria in CD8⁺ T cells as in **Fig. 1E**. **(D-E)** Seahorse extracellular flux analysis of OCR **(D)** and ECAR **(E)** of naive WT or C1qbp-tKO CD8⁺ T cells (n = 11 (**D**) or 7 (**E**) wells per group). Each symbol represents an individual well of cells, small horizontal lines indicate the mean (±s.d.). ****P < 0.0001(two-tailed unpaired Student's t-test). Data are representative of two (**C**) or three (**B**, **D**, **E**) independent experiments (error bars, s.d.).

Fig. S2

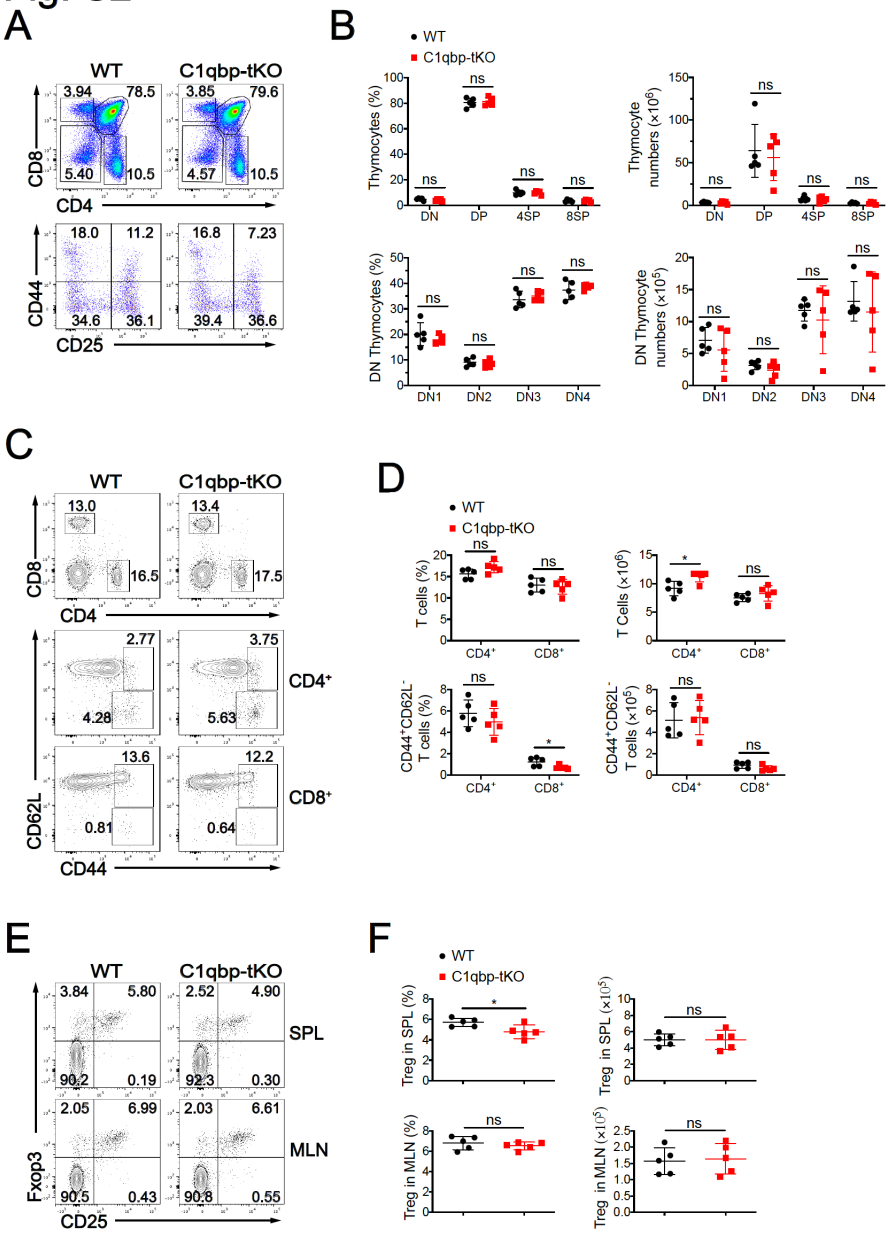
A
WT
C1qbp-tKO
CD8
CD4
CD44
CD25
B
WT
C1qbp-tKO
Thymocytes (%)
Thymocyte numbers (×10^6)
DN Thymocytes (%)
DN Thymocyte numbers (×10^5)
DN
DP
4SP
8SP
DN1
DN2
DN3
DN4
ns
C
CD62L
CD4+
CD8+
D
T cells (%)
T Cells (×10^6)
CD44+CD62L- T cells (%)
CD44+CD62L- T cells (×10^5)
*
E
SPL
MLN
Fxop3
F
Treg in SPL (%)
Treg in SPL (×10^5)
Treg in MLN (%)
Treg in MLN (×10^5)

Fig. S2. C1qbp is dispensable for T cell development and peripheral homeostasis. **(A)** Flow cytometry of total thymocytes (top row) and double negative (DN) thymocytes (bottom row) from WT and C1qbp-tKO mice. **(B)** Frequency and number of thymocyte subpopulations (top row) and DN subpopulations (bottom row) cells from mice as in **A** (n = 5 per group). **(C)** Flow cytometry of total splenocytes (top row) and splenic $CD4^+$ (middle row) and splenic $CD8^+$ (bottom row) T cells from mice as in **A**. **(D)** Frequency and total number of splenic $CD4^+$ or $CD8^+$ (among splenocytes) (top row), $CD44^+CD62L^-$ effector memory $CD4^+$ or $CD8^+$ T cells (among splenic $CD4^+$ or $CD8^+$ T cells) (bottom row) cells from mice as in **A** (n = 5 per group). **(E)** Flow cytometry of $CD4^+$ T cells in spleen (SPL) (top row) and mesenteric LN (MLN) (bottom row) from mice as in **A**. **(F)** Frequency (among $CD4^+$ T cells) and number of $CD25^+$ $Foxp3^+$ Treg cells from mice as in **A** (n = 5 per group). Each symbol represents an individual mouse, small horizontal lines indicate the mean (±s.d.). *$P < 0.05$; ns, not significant (two-tailed unpaired Student's t-test). Data are representative of three independent experiments (error bars, s.d.).

Fig. S3

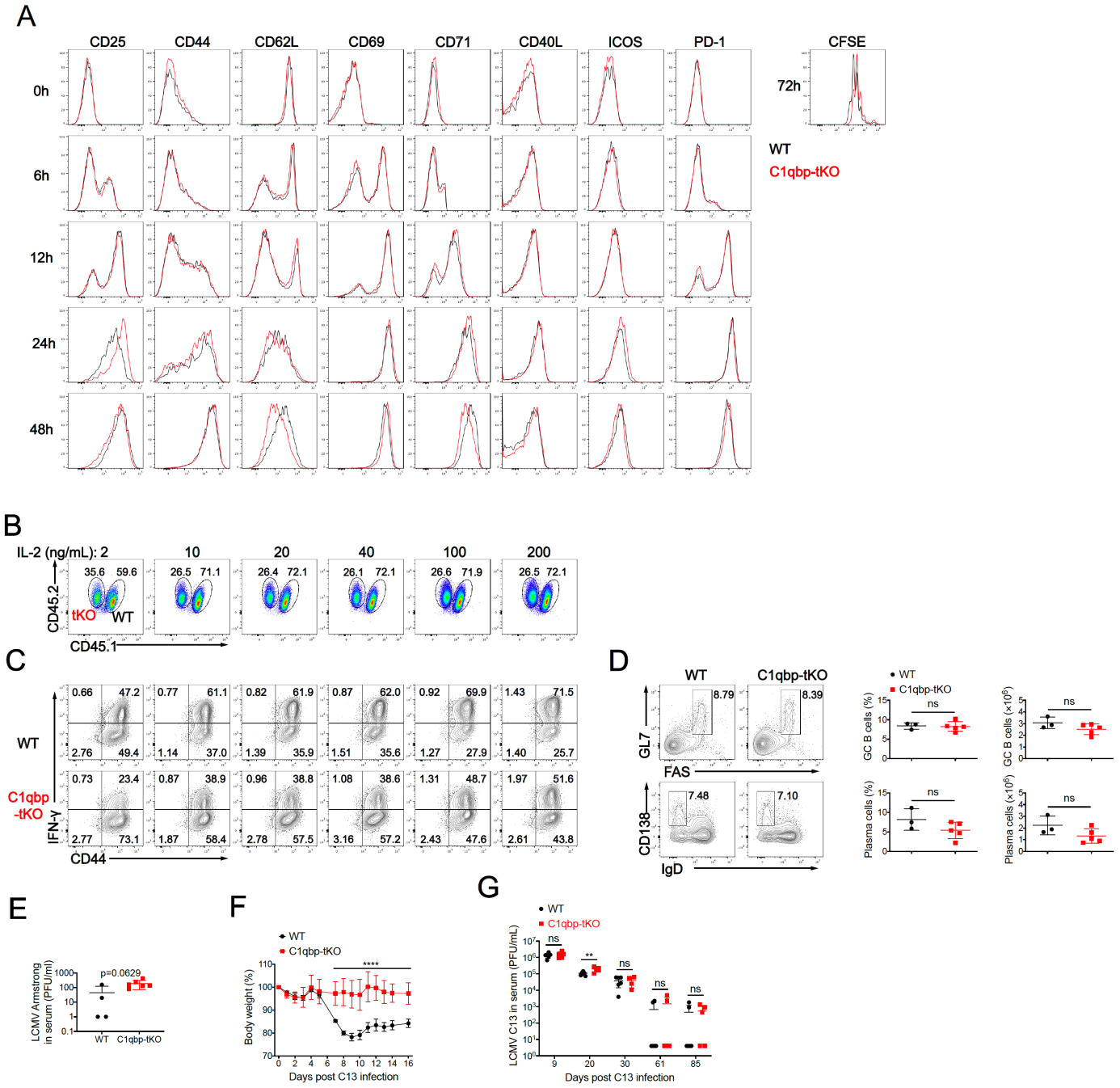
A
CD25
CD44
CD62L
CD69
CD71
CD40L
ICOS
PD-1
CFSE
0h
6h
12h
24h
48h
72h
WT
C1qbp-tKO
B
IL-2 (ng/mL): 2
10
20
40
100
200
CD45.2
CD45.1
tKO
WT
C
WT
C1qbp -tKO
IFN-γ
CD44
D
WT
C1qbp-tKO
GL7
FAS
CD138
IgD
GC B cells (%)
GC B cells (×10^6)
Plasma cells (%)
Plasma cells (×10^6)
ns
E
LCMV Armstrong in serum (PFU/ml)
p=0.0629
F
Body weight (%)
Days post C13 infection
****
G
LCMV C13 in serum (PFU/mL)
Days post C13 infection
**

Fig. S3. C1qbp is required for effector CD8$^+$ T cell response. (A) Flow cytometry of CD8$^+$ T cells purified from WT or C1qbp-tKO mice, stimulated with plate-bound anti-CD3ε (1 μg/mL) and anti-CD28 (1 μg/mL) for indicated hours. The expression of indicated markers was analyzed by flow cytometry (left). Proliferation of CD8$^+$ T cells was indicated by flow cytometry of CFSE dilution (right) (n = 2). **(B-C)** CD8$^+$ T cells purified from WT and C1qbp-tKO mice were 1:1 mixed and stimulated with plate-bound anti-CD3ε (1 μg/mL) and anti-CD28 (1 μg/mL) for 2 days, and then cultured with IL-2 of indicated concentration for 4 days. The proportion (**B**) and expression of IFN-γ (**C**) of the cells were analyzed by flow cytometry (n = 2). **(D)** Flow cytometry of total splenic B220$^+$ B cells from WT and C1qbp-tKO mice at day 8 after infection with LCMV Armstrong. Frequency and number of FAS$^+$ GL7$^+$ GC B cells (top row) and CD138$^+$ IgD$^-$ plasma cells (bottom row). (WT, n = 3; C1qbp-tKO, n = 5). **(E)** The viral titers in the serum of WT and C1qbp-tKO mice were determined as described in Methods at day 5 after infection with LCMV Armstrong (n = 4 or 6 per group). **(F-G)** WT and C1qbp-tKO mice were infected intravenously with LCMV Clone 13. Body weight **(F)** and viral titers in the serum **(G)** were determined at indicated days after infection (n = 6 per group). Each symbol represents an individual mouse, small horizontal lines indicate the mean (±s.d.). **P < 0.01, ****P < 0.0001; ns, not significant (two-tailed unpaired Student's t-test). Data are representative of two **(E-G)** or three **(A-D)** independent experiments (error bars, s.d.).

Fig. S4

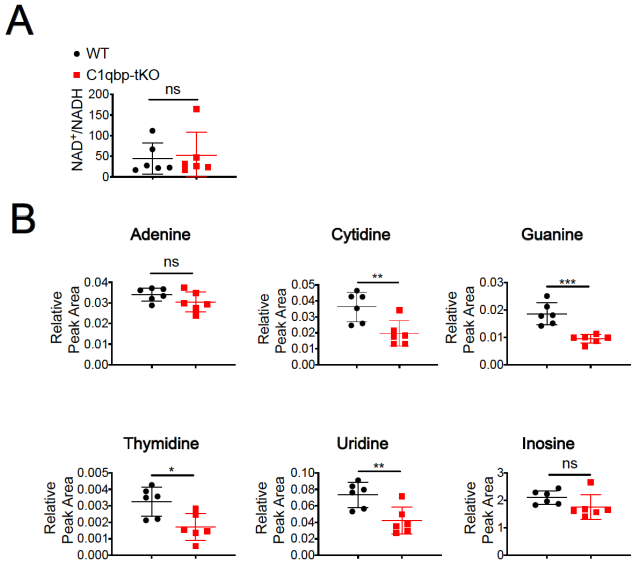

Fig. S4. *C1qbp* deficiency results in dysregulated metabolites in activated CD8$^+$ T cells. (A-B) Metabolomic analysis of WT and *C1qbp*-deficient P14 CD8$^+$ T cells as in Fig. 4E. **(A)** The ratio of NAD$^+$/NADH in WT and *C1qbp*-deficient P14 cells. **(B)** Relative abundance of nucleotides. (n = 6 per group). Each symbol represents an individual mouse, small horizontal lines indicate the mean (±s.d.). *P < 0.05, **P < 0.01 and ***P < 0.001; ns, not significant (two-tailed unpaired Student's t-test). Data are representative of two independent experiments (error bars, s.d.).

Fig. S5

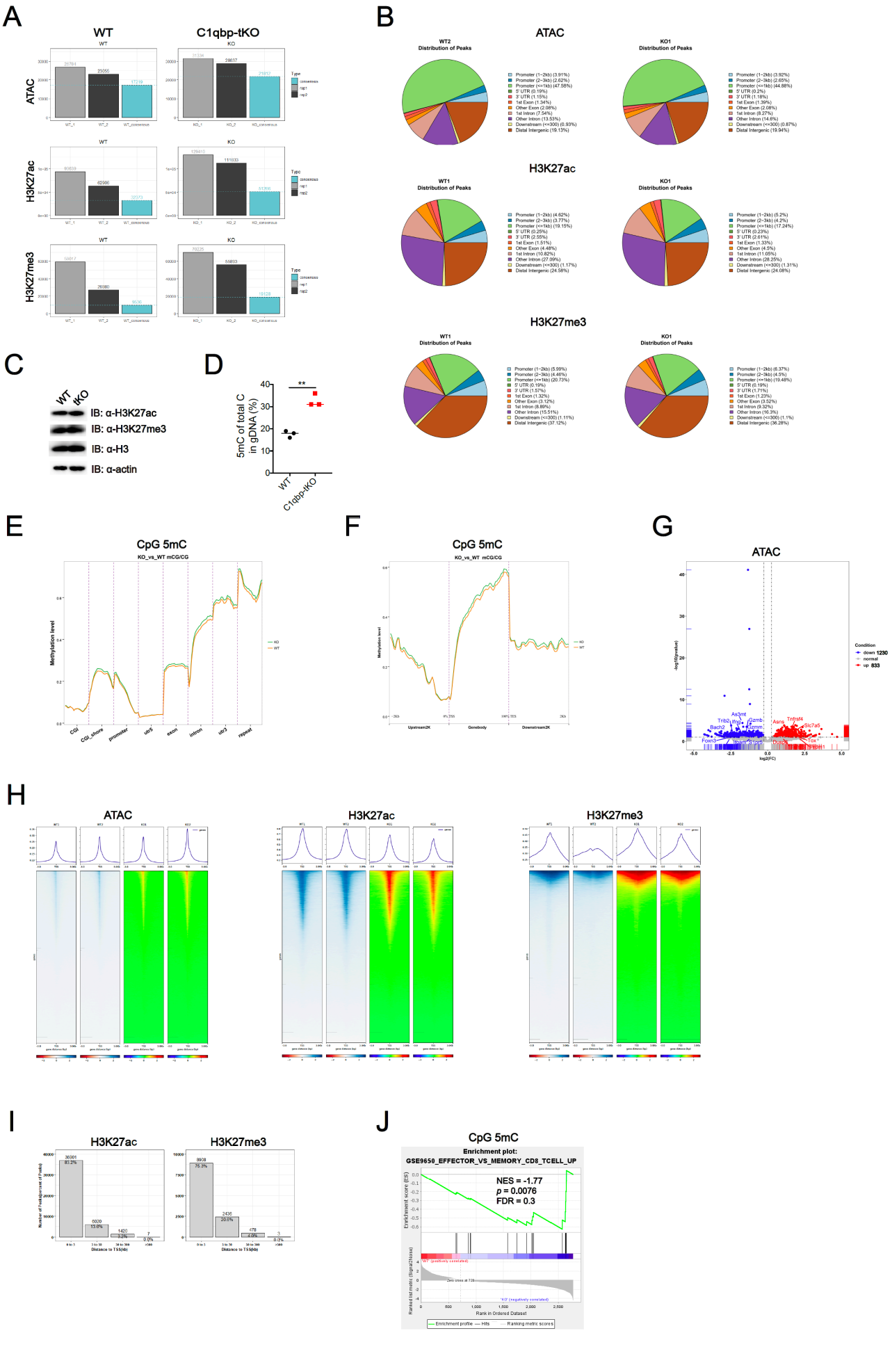
A
WT
C1qbp-tKO
ATAC
H3K27ac
H3K27me3
B
ATAC
H3K27ac
H3K27me3
C
WT
tKO
IB: α-H3K27ac
IB: α-H3K27me3
IB: α-H3
IB: α-actin
D
5mC of total C in gDNA (%)
WT
C1qbp-tKO
E
CpG 5mC
KO_vs_WT mCG/CG
Methylation level
F
CpG 5mC
KO_vs_WT mCG/CG
G
ATAC
H
ATAC
H3K27ac
H3K27me3
I
H3K27ac
H3K27me3
J
CpG 5mC
Enrichment plot:
GSE9650_EFFECTOR_VS_MEMORY_CD8_TCELL_UP
NES = -1.77
p = 0.0076
FDR = 0.3

Fig. S5. Altered epigenetic profiling in activated *C1qbp*-deficient CD8$^+$ T cells. (A) Bar graph showing the number of consensus peaks (blue) shared between replicates (light gray and dark gray) of accessible regions from ATAC-seq (top), H3K27ac (middle) and H3K27me3 (bottom) depositions from CUT&Tag datasets of WT and *C1qbp*-deficient P14 CD8$^+$ T cells as in Fig. 5A. **(B)** Distribution of accessible regions (ATAC-seq) (top), and H3K27ac (middle) and H3K27me3 (bottom) depositions in genomic regions of WT and *C1qbp*-deficient P14 CD8$^+$ T cells as in Fig. 5A. **(C)** Immunoblot analysis for H3K27ac and H3K27me3 in WT and *C1qbp*-deficient P14 CD8$^+$ T cells as in Fig. 5A. **(D)** Percentage of 5-methylcytosine of total cytosine in genomic DNA of WT and *C1qbp*-deficient P14 CD8$^+$ T cells as in Fig. 5A ($n = 3$ per group). Each symbol represents an individual mouse, small horizontal lines indicate the mean (±s.d.). $^{**}P < 0.01$ (two-tailed unpaired Student's t-test). Data are representative of two independent experiments (error bars, s.d.) **(E-F)** CpG 5mC level at different region of genes **(E)**, and around the TSS and transcriptional end site (TES) **(F)** in cells as in Fig. 5A. **(G)** Volcano plot illustrating differentially accessible chromatin regions (DARs) between WT and *C1qbp*-deficient P14 CD8$^+$ T cells as in Fig. 5A. **(H)** Deposition of accessible regions (ATAC-seq) (left), H3K27ac (middle) and H3K27me3 (right) centered on TSS ± 3 kb in WT and *C1qbp*-deficient CD8$^+$ T cells as in Fig. 5A. **(I)** Consensus peaks in (**A**) were annotated to the TSS of the nearest gene. Bar plots show the number of regions falling within a given distance for DMRs of H3K27ac (left) and H3K27me3 (right) regions. **(J)** GSEA of indicated signature genes from the ranked list of CpG 5mC DMRs in cells as in Fig. 5A. Data shown contain the union of significant consensus peaks identified across two independent biological replicates.

Fig. S6

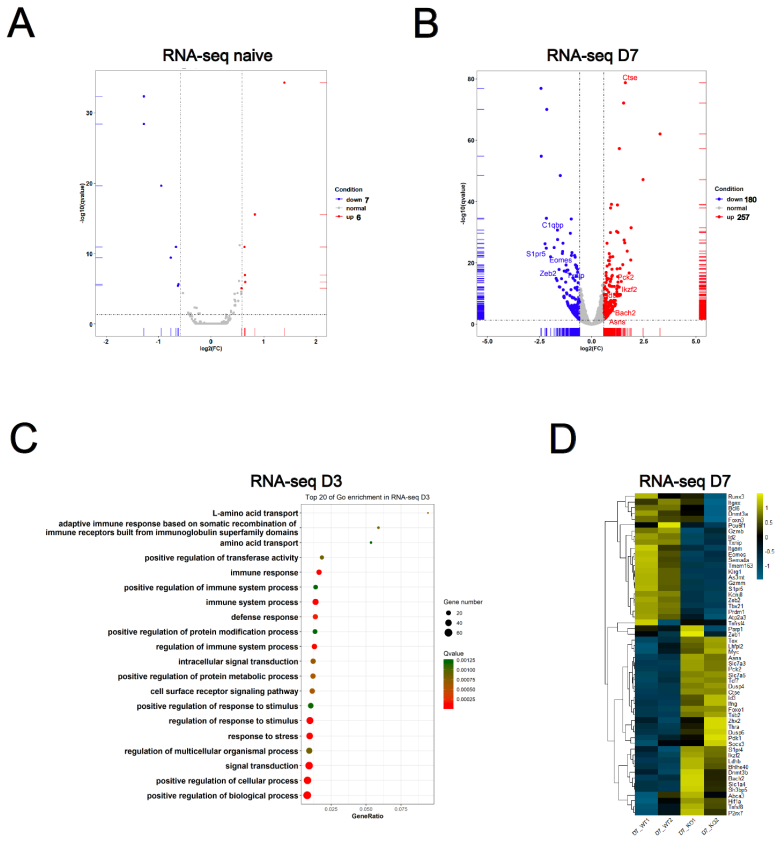

Fig. S6. *C1qbp* deficiency impedes transcriptional program of effector CD8$^+$ T cells. **(A-B)** Volcano plots illustrating DEGs in the naïve WT and *C1qbp*-deficient CD8$^+$ T cells (**A**) and those from recipient mice at day 7 (**B**) after infection with LCMV Armstrong (n = 2 per group). **(C)** GO analysis of DEGs in WT and *C1qbp*-deficient CD8$^+$ T cells from recipient mice at day 3 after infection with LCMV Armstrong. **(D)** Heatmap of differentially expressed effector-signature and memory-signature genes in WT and *C1qbp*-deficient CD8$^+$ T cells from recipient mice at day 7 after infection with LCMV Armstrong.

Fig. S7

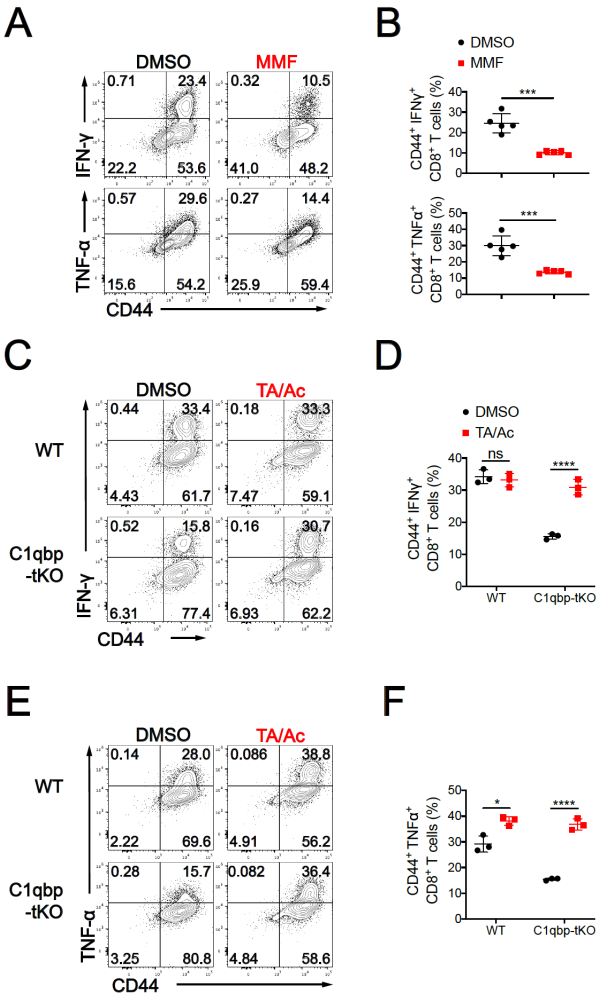
A
DMSO
MMF
IFN-γ
TNF-α
CD44
0.71
23.4
22.2
53.6
0.32
10.5
41.0
48.2
0.57
29.6
15.6
54.2
0.27
14.4
25.9
59.4
B
DMSO
MMF
CD44+ IFNγ+ CD8+ T cells (%)
CD44+ TNFα+ CD8+ T cells (%)
***
C
DMSO
TA/Ac
WT
C1qbp -tKO
IFN-γ
CD44
0.44
33.4
4.43
61.7
0.18
33.3
7.47
59.1
0.52
15.8
6.31
77.4
0.16
30.7
6.93
62.2
D
DMSO
TA/Ac
CD44+ IFNγ+ CD8+ T cells (%)
ns
****
WT
C1qbp-tKO
E
DMSO
TA/Ac
WT
C1qbp -tKO
TNF-α
CD44
0.14
28.0
2.22
69.6
0.086
38.8
4.91
56.2
0.28
15.7
3.25
80.8
0.082
36.4
4.84
58.6
F
CD44+ TNFα+ CD8+ T cells (%)
*
****
WT
C1qbp-tKO

Fig. S7. The production of effector cytokine in CD8$^+$ T cells is affected by *in vitro* treatment of Fumarate or TA/Ac. (A-B) WT naïve CD8$^+$ T cells were treated with vehicle (DMSO) or MMF in culture medium for 1 day. Then cells were stimulated with plate-bound anti-CD3ε (1 μg/mL) and anti-CD28 (1 μg/mL) in the presence of IL-2 for 3 days and cytokines were test. (**A**) Flow cytometry of IFN-γ (top row) or TNF-α (bottom row) producing CD8$^+$ T cells treated with DMSO (left) or MMF (right). **(B)** Frequency of CD44$^+$ IFN-γ$^+$ CD8$^+$ T cells (top row) and CD44$^+$ TNF-α$^+$ CD8$^+$ T cells (bottom row) as in **A** (n = 5 per group). **(C-F)** Naïve CD8$^+$ T cells purified from WT or C1qbp-tKO mice were stimulated with plate-bound anti-CD3ε (1 μg/mL) and anti-CD28 (1 μg/mL) in the presence of IL-2 for 2 days. Then cells were resuspended and treated with vehicle (DMSO) or TA/Ac in culture medium containing IL-2 for 1 day. After treatment, cells were resuspended and cultured in medium with IL-2 for another 2 days. (**C, E**) Flow cytometry of IFN-γ (**C**) and TNF-α (**E**) producing CD8$^+$ T cells treated with DMSO (left) or TA/Ac (right). **(D, F)** Frequency of CD44$^+$ IFN-γ$^+$ CD8$^+$ T cells (**D**) and CD44$^+$ TNF-α$^+$ CD8$^+$ T cells (**F**) as in **C** (n = 3 per group). Small horizontal lines indicate the mean (±s.d.). *P < 0.05, **P < 0.01, ***P < 0.001 and ****P < 0.0001; ns, not significant (two-tailed unpaired Student's t-test). Data are representative of two independent experiments (error bars, s.d.).

Fig. S8

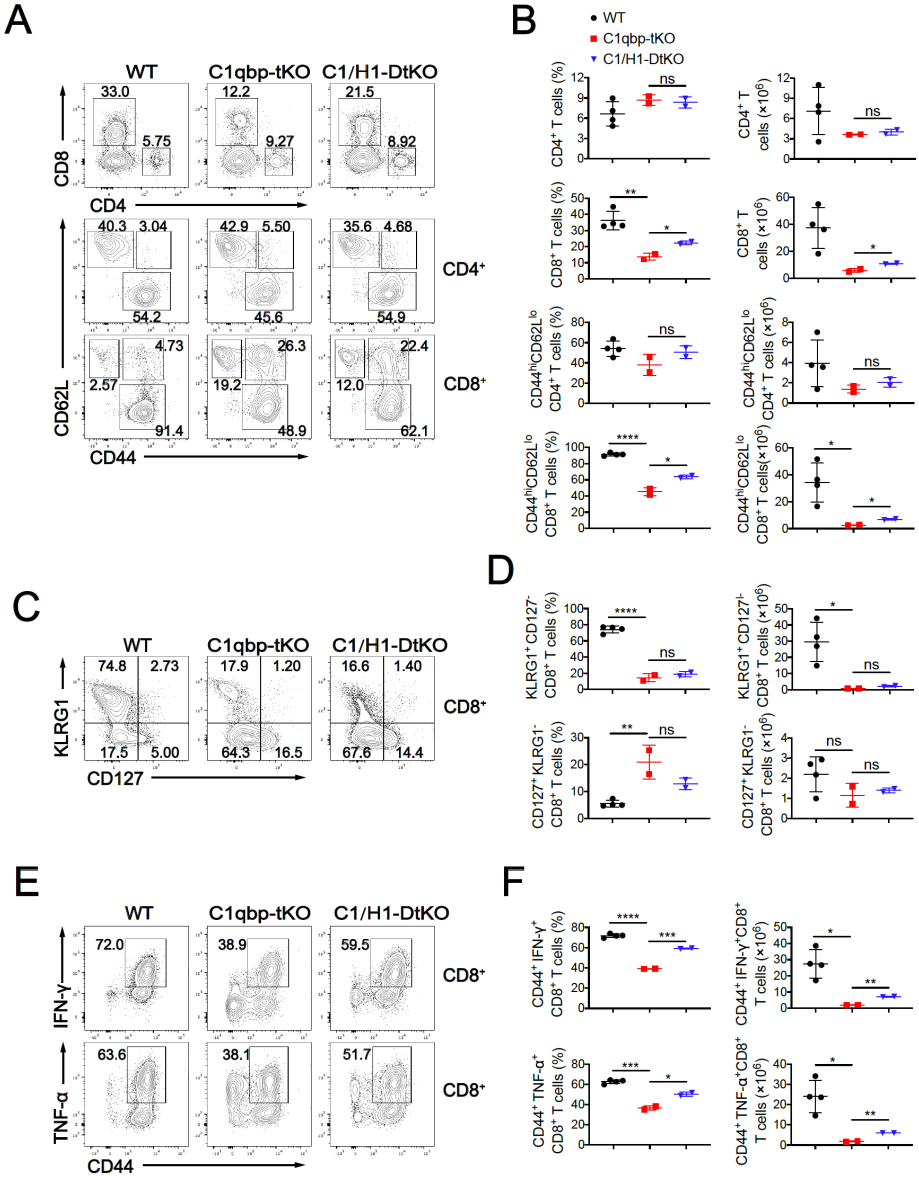
A
WT
C1qbp-tKO
C1/H1-DtKO
CD8
CD4
33.0
5.75
12.2
9.27
21.5
8.92
CD62L
CD44
40.3
3.04
54.2
42.9
5.50
45.6
35.6
4.68
54.9
CD4+
4.73
2.57
91.4
26.3
19.2
48.9
22.4
12.0
62.1
CD8+
B
WT
C1qbp-tKO
C1/H1-DtKO
CD4+ T cells (%)
CD4+ T cells (×10^6)
CD8+ T cells (%)
CD8+ T cells (×10^6)
CD44hiCD62Llo CD4+ T cells (%)
CD44hiCD62Llo CD4+ T cells (×10^6)
CD44hiCD62Llo CD8+ T cells (%)
CD44hiCD62Llo CD8+ T cells(×10^6)
ns
*
**
****
C
WT
C1qbp-tKO
C1/H1-DtKO
KLRG1
CD127
74.8
2.73
17.5
5.00
17.9
1.20
64.3
16.5
16.6
1.40
67.6
14.4
CD8+
D
KLRG1+CD127- CD8+ T cells (%)
KLRG1+CD127- CD8+ T cells (×10^6)
CD127+KLRG1- CD8+ T cells (%)
CD127+KLRG1- CD8+ T cells (×10^6)
E
WT
C1qbp-tKO
C1/H1-DtKO
IFN-γ
TNF-α
CD44
72.0
38.9
59.5
CD8+
63.6
38.1
51.7
CD8+
F
CD44+ IFN-γ+ CD8+ T cells (%)
CD44+ IFN-γ+CD8+ T cells (×10^6)
CD44+ TNF-α+ CD8+ T cells (%)
CD44+ TNF-α+CD8+ T cells (×10^6)
***

Fig. S8. *Hif1a* deficiency partially restores defective effector CD8$^+$ T cells in C1qbp-tKO mice. (A) Flow cytometry of total splenocytes (top row) and splenic CD4$^+$ (middle row) and splenic CD8$^+$ (bottom row) T cells from WT, C1qbp-tKO and C1/H1-DtKO mice at day 8 after infection with LCMV Armstrong. **(B)** Frequency and total number of splenic CD4$^+$ or CD8$^+$ (among splenocytes), CD44^{hi}CD62L^{lo} effector CD4$^+$ or CD8$^+$ T cells (among splenic CD4$^+$ or CD8$^+$ T cells) cells from mice as in **A**. **(C)** Flow cytometry of splenic CD8$^+$ T cells from mice as in **A**. **(D)** Frequency (among CD8$^+$ T cells) and total number of KLRG1$^+$ effector (top row) or CD127$^+$ memory precursor (bottom row) CD8$^+$ T cells in spleens of mice as in **A**. **(E)** Flow cytometry of splenic CD8$^+$ T cells from mice as in **A**. **(F)** Frequency (among CD8$^+$ T cells) and total number of IFN-γ^+ (top row) or TNF-α^+ (bottom row) effector CD8$^+$ T cells in spleens of mice as in **A**. (WT, n = 4; C1qbp-tKO, n = 2; C1/H1-DtKO, n = 2) Each symbol represents an individual mouse, small horizontal lines indicate the mean (±s.d.). *P < 0.05, **P < 0.01, ***P < 0.001 and ****P < 0.0001; ns, not significant (two-tailed unpaired Student's t-test). Data are representative of three independent experiments (error bars, s.d.).

Fig. S9

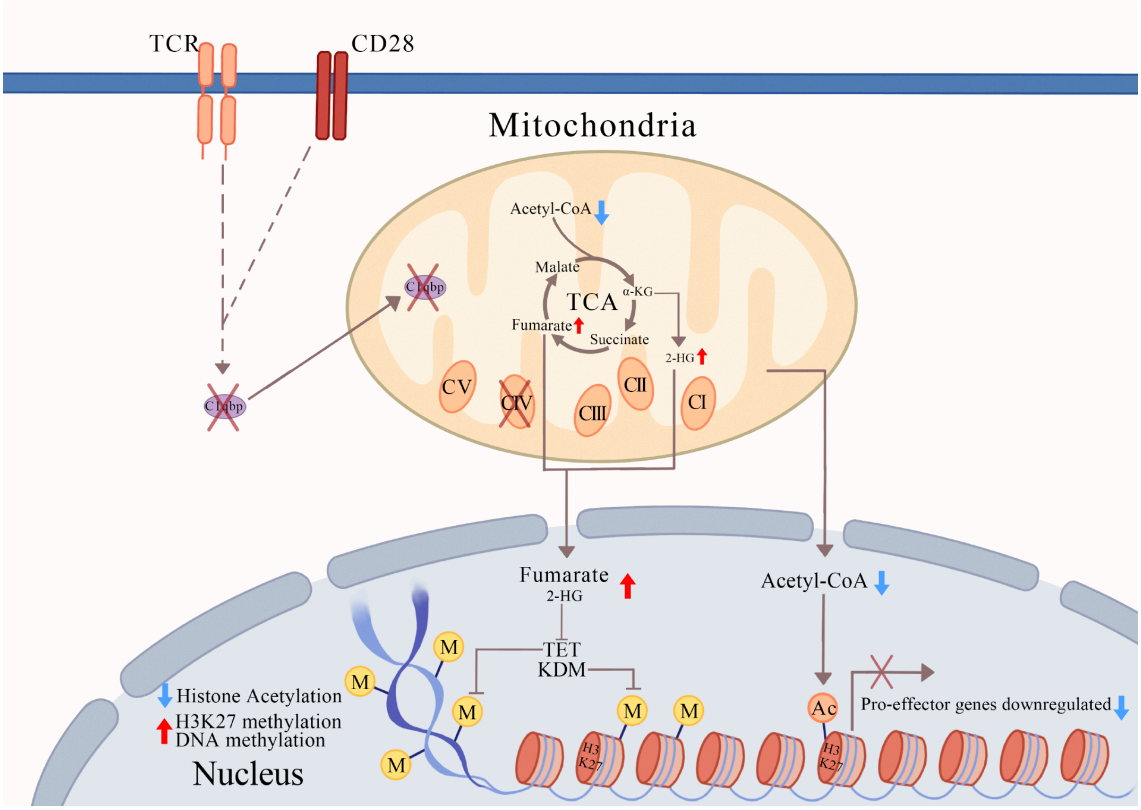

Fig. S9. Proposed model for the role of C1qbp in differentiation of effector CD8$^+$ T cells. C1qbp expression is induced upon T cell activation. *C1qbp* deficiency leads to the disorder of mitochondrial metabolism in activated CD8$^+$ T cells, resulting in accumulation of fumarate and 2-HG as well as decrease of acetyl-CoA. Elevated fumarate and 2-HG could inhibit both TET-mediated DNA demethylation and KDM-mediated histone demethylation, while acetyl-CoA is donor for acetyl group of histone acetylation. Consequently, hypoacetylation of H3K27 and hypermethylation of H3K27 and CpG sites, are associated with transcriptional downregulation of effector signature genes. All of these eventually impair the differentiation of effector CD8$^+$ T cells.

Table S1. Mass Spectrometry analysis of mitochondrial proteins in WT and *C1qbp*-deficient CD8$^+$ T cells after *in vitro* activation. Naïve CD8$^+$ T cells purifies from WT and C1qbp-tKO mice were stimulated *in vitro* with plate-bound anti-CD3ε (3 μg/mL) and anti-CD28 (3 μg/mL) for 2 days. Quantification of protein levels of mitochondrial proteins in activated WT or C1qbp-tKO CD8$^+$ T cells was performed by Mass spectrum.

Table S2. Metabolomic analysis of activated WT and *C1qbp*-deficient P14 CD8$^+$ T cells after LCMV infection. Activated WT and *C1qbp*-deficient P14 CD8$^+$ T cells were sorted from B6.SJL recipient mice respectively, at day 5 after infection with LCMV Armstrong. Metabolomic analysis of activated WT and *C1qbp*-deficient P14 CD8$^+$ T cells was performed by Mass spectrum.